Abnormalities of structural brain connectivity in pediatric brain tumor survivors

Adeoye Oyefiade[©], Iska Moxon-Emre, Kiran Beera, Eric Bouffet[©], Michael Taylor, Vijay Ramaswamy, [©]Suzanne Laughlin, Jovanka Skocic, and Donald J. Mabbott

Neurosciences and Mental Health, The Hospital for Sick Children, Toronto, Ontario, Canada (A.O., K.B., D.M.); Campbell Family Mental Health Research Institute, Centre for Addiction and Mental Health, Toronto, Ontario, Canada (I.M.-E., J.S.); Division of Hematology/Oncology, The Hospital for Sick Children, Toronto, Ontario, Canada (E.B., V.R., D.M.); Division of Neurosurgery, The Hospital for Sick Children, Toronto, Ontario, Canada (M.T.); Division of Radiology, The Hospital for Sick Children, Toronto, Ontario, Canada (S.L.); Department of Psychology, University of Toronto, Toronto, Ontario, Canada (A.O., D.M.)

Corresponding Author: Donald J. Mabbott, PhD, Neurosciences and Mental Health Program, The Hospital for Sick Children, Peter Gilgan Centre for Research and Learning (PGCRL), 686 Bay Street, Toronto, ON M5G0A4, Canada (donald.mabbott@sickkids.ca).

Abstract

Background. Pediatric brain tumor survivors are at an increased risk for white matter (WM) injury. However, damage to whole-brain structural connectivity is unelucidated. The impact of treatment on WM connectivity was investigated.

Methods. Whole-brain WM networks were derived from diffusion tensor imaging data acquired for 28 irradiated patients (radiotherapy, RT) (mean age = 13.74 ± 3.32 years), 13 patients not irradiated (No RT) (mean age = 12.57 ± 2.87), and 41 typically developing children (TDC) (mean age = 13.32 ± 2.92 years). Differences in network properties were analyzed using robust regressions.

Results. Participation coefficient was lower in both patient groups (RT: adj. $P = .015$; No RT: adj. $P = .042$). Compared to TDC, RT had greater clustering (adj. $P = .015$), local efficiency (adj. $P = .003$), and modularity (adj. $P = .000003$). WM traced from hubs was damaged in patients: left hemisphere pericallosal sulcus (FA [$F = 4.97$; $q < 0.01$]; MD [$F = 11.02$; $q < 0.0001$]; AD [$F = 10.00$; $q < 0.0001$]; RD [$F = 8.53$; $q < 0.0001$]), right hemisphere pericallosal sulcus (FA [$F = 8.87$; $q < 0.0001$]; RD [$F = 8.27$; $q < 0.001$]), and right hemisphere parietooccipital sulcus (MD [$F = 5.78$; $q < 0.05$]; RD [$F = 5.12$; $q < 0.05$]).

Conclusions. Findings indicate greater segregation of WM networks after RT. Intermodular connectivity was lower after treatment with and without RT. No significant network differences were observed between patient groups. Our results are discussed in the context of a network approach that emphasizes interactions between brain regions.

Key Points

- Whole-brain WM networks are highly disconnected in childhood brain tumor survivors.
- Highly connected brain regions vulnerable to injury following brain tumor treatment.
- Deficits in WM microstructure are correlated with disruptions in network connectivity.

Childhood neurologic studies are increasingly conceptualizing pediatric brain injury as a disorder of brain connectivity.[1] This paradigm shift is rooted in theories of cognition which suggest that higher-order cognitive processes emerge from interactions between distributed brain regions. Emerging evidence suggests that whole-brain white matter (WM) connectivity is sensitive to changes in behavior resulting from injury.[2,3] We extend this work by investigating the effects of treatment on whole-brain WM connectivity in children diagnosed with a brain tumor.

Treatment for a pediatric brain tumor (PBT) may require neurosurgery, cranial radiotherapy (RT), adjuvant chemotherapy, or a combination. RT is a known to be risk factor for significant

Importance of the Study

Prior work has demonstrated that brain tumor treatment is neurotoxic and disruptive to white matter microstructure. While injury to individual white matter tracts is correlated to specific deficits, relations to changes in behaviors have not been studied. Human behavior emerges from interactions between distributed brain regions embedded within a whole-brain white matter network. We found that pediatric brain tumor treatment is related to highly disconnected whole-brain white matter networks in survivors. Highly connected regions are disproportionately affected whereas other regions remained unchanged. These findings have been demonstrated in other neuropsychiatric and neurodevelopmental populations; this work is the first to demonstrate these changes in pediatric brain tumor survivors. Our results may help explain treatment-induced deficits in cognitive and behavioral outcome via impact on whole-brain white matter connectivity.

WM injury because diffuse irradiation of healthy brain tissue impacts WM development.[4] Lower RT dose and field volume result in greater sparing of WM in PBT survivors.[5] Neurosurgery is associated with cognitive risk because of damage to supratentorial WM.[6] Broadly speaking, chemotherapy treatment confers less risk for injury than RT, though chemotherapy-only regimens are linked with poorer outcomes in PBT survivors.[7]

Network analysis of large-scale neuroimaging data has enabled a characterization of the dense integrative network of WM connections linking the entire brain.[8] We can now evaluate the extent to which brain regions are connected into an integrated whole (*integration*) or are distinguishable (*segregation*).[8] It is also possible to describe the importance of a brain region to network connectivity (*centrality*), where highly connected hubs facilitate integrative connectivity between anatomically unconnected brain regions.[9] Connectivity studies show that developmental increases in network integration are closely aligned with the acquisition of complex skills in childhood.[10,11] Alterations to the structural connectome in the form of greater network segregation and compromised modular structure have been identified in several clinical populations[12–14] and are associated with worse cognitive and behavioral outcomes.[15,16]

In the current study, we analyzed diffusion tensor imaging (DTI) data from PBT survivors and an age/sex-matched sample of typically developing children (TDC). DTI provides reliable but indirect information about tissue microstructure by quantifying the translational displacement of water molecules across fatty tissue.[17,18] PBT survivors exhibit diffuse WM injury.[19–21] As such, the primary hypothesis of our study is that treatment with RT will result in greater compromise to whole-brain WM networks. It was also hypothesized that larger RT dose and field would result in greater network compromise.

Materials and Methods

Study Demographics

Twenty-eight children treated with RT (RT) (mean age = 13.74 ± 3.32 years, 39% female), 13 children treated without RT (No RT) (mean age = 12.57 ± 2.87 years, 54% female), and 41 matched TDC (mean age = 13.32 ± 2.92 years, 49% female) were recruited at the Hospital for Sick Children (SickKids) in Toronto, Canada. The TDC group was selected if they had no premorbid history of developmental delay, learning disability, psychiatric/neurological disorder, and traumatic brain injury. Informed written consent, or assent and consent from a parent/caregiver for younger children was obtained by trained personnel who reviewed all consent forms and answered all questions prior to study participation. Access to participant medical databases was approved by the hospital's research ethics board. Tumor diagnoses and clinical variables are presented in Table 1. The RT group received either a standard (30.6–39.4 Gy) or reduced craniospinal RT dose (18–23.4 Gy), plus a boost volume to the posterior fossa or the tumor bed. Treatment stratification resulted in 4 treatment combinations: reduced craniospinal RT plus a tumor bed boost, reduced craniospinal RT plus a posterior fossa boost, standard craniospinal RT plus a tumor bed boost, and standard craniospinal RT plus a posterior fossa boost. In all cases, total RT dose delivered was 45–55.4 Gy.

Image Acquisition and T1 Image Processing

Magnetic resonance images were acquired using a Siemens 3 Tesla whole-body scanner with a twelve channel head coil. The scanning parameters were a 3-dimensional T1 magnetization prepared 180 degrees radiofrequency pulse with a rapid gradient echo (MPRAGE) Grappa 2 protocol (TE/TR = 3.91/2300 ms, 160 contiguous axial slices, flip angle = 90°, 256 × 224 matrix, FOV = 256 × 224 mm, voxel size = 1 mm ISO) and a single-shot spin echo diffusion-weighted protocol (30 directions, b = 1000 s/mm^2, TE/TR = 90/9000 ms, 70 contiguous axial slices, flip angle = 90°, 122 × 122 matrix interpolated to 244 × 244, FOV = 244 × 244 mm, voxel size = 2 mm ISO, encoding direction = A/P).

Cortical reconstruction and volumetric segmentation of T1 images were performed as previously described.[22] The cortical surface was subdivided into 148 distinct regions according to a well-validated atlas[23] (Supplementary Table 1). Estimated intracranial volume (ICV) was obtained to normalize brain network metrics.

Table 1. Demographic and clinical characteristics of all participants in the study

	Healthy controls (41)	Radiated brains (28)	Surgery only (13)	p
Sex				
Males (%)	21 (51%)	17 (61%)	6 (46%)	.49
Handedness				
Right hand (%)	39 (95%)	22 (79%)	10 (77%)	.07
Age at study (y)				
Mean (±SD)	13.32 ± 2.92	13.74 ± 3.32	12.57 ± 2.87	.55
Range	6.66–18.94	7.50–18.98	9.36–17.49	
Age at diagnosis (y)				
Mean (±SD)	—	7.05 ± 2.39	6.79 ± 4.22	.91
Range	—	3.00–11.60	2.11–16.8	
Time since diagnosis (y)				
Mean (±SD)	—	5.79 ± 3.22	6.69 ± 3.88	.42
Tumor type				
Medulloblastoma	—	26	1	—
Pilocytic astrocytoma	—	—	11	—
Ependymoma	—	2	1	—
Surgical resection				
Gross total (%)	—	22 (79%)	10 (77%)	.89
Radiation therapy[a]				
Reduced dose CSR	—	18	—	
Posterior fossa boost	—	2	—	
Tumor bed boost	—	16	—	
Standard dose CSR	—	9	—	
Posterior fossa boost	—	4	—	
Tumor bed boost	—	5	—	
Chemotherapy protocol[b,c]				
A	—	6 (21%)	—	
B	—	3 (11%)	—	
C	—	13 (46%)	—	
D	—	1 (4%)	—	
E	—	1 (4%)	—	
Perioperative complications				
Hydrocephalus	—	21 (71%)	7 (54%)	.12
Motor deficits	—	22 (79%)	6 (46%)	.11
Mutism	—	10 (36%)	2 (15%)	.19

CSR, craniospinal radiation.
[a]Treatment information missing for 1 patient.
[b]Chemotherapy protocols available for only 24 patients.
[c]Chemotherapy protocols and associated agents are as follows: A: CCG 9961 (Vincristine, Lomustine, Cisplatin); B: POG 9631 (Etoposide, Cisplatin, Cyclophosphamide, Vincristine); C: SJMB03 (Vincristine, Cisplatin, Cyclophosphamide, Amifostine); D: COG 99703 (Vincristine, Cisplatin, Cyclophosphamide, Etoposide); E: ACNS 0331 (Lomustine, Cisplatin, Vincristine, Cyclophosphamide).

Diffusion-Weighted Image Preprocessing and Probabilistic Tractography

Diffusion-weighted images were corrected for eddy current distortions, motion artifacts, and B1 inhomogeneities.[24] WM modeling and fiber tractography was completed using standard pipeline from the MRtrix3 package Version 3.0.0.[25]

Network Construction

Streamline connectomes: T1 images were parcellated into distinct cortical regions to define the nodes of the structural network (Figure 1). Probabilistic streamlines connecting all node pairs were mapped to form the edges of the network. An edge was defined as the number of

streamlines connecting any pair of nodes. A 148 × 148 symmetric matrix was constructed representing the structural connectivity of the whole brain. Unlike deterministic tractography, mapping probabilistic streamlines increases the likelihood of spurious connections, therefore it was necessary to apply a thresholding scheme to minimize the occurrence of such connections in the connectivity matrix. Choosing a threshold is challenging, as a priori assumptions about network properties need to be made in order to decide on thresholding criteria.[26] To overcome this issue, we calculated network measures across a range of thresholds and summarized the computed measures by calculating the area under the curve for each network measure.[27] A threshold range between 0.05 and 0.35 at intervals of 0.01 was applied to each structural network. This network range allowed us to derive sparse and fully connected networks. Thresholded networks were binarized prior to calculating network measures.

Network Measures

Network measures were calculated in MATLAB Version 2019b using scripts from the Brain Connectivity Toolbox (brain-connectivity-toolbox.net)[8] and GRETNA software.[28] Each binarized network was considered as a graph G with

N nodes. A summary of network measures is provided in Supplementary Materials.

Measures of network integration, segregation, and centrality are denoted below:

INTEGRATION: characteristic path length, global efficiency
SEGREGATION: clustering coefficient, local efficiency, modularity
CENTRALITY: degree centrality, participation coefficient, betweenness centrality.

Statistical Analysis

Statistical analyses and *P*-value hypothesis testing were completed using the R Statistical software package Version 3.6.0. (http://www.r-project.org). Group differences were calculated using 1-way analysis of variance models.

Group differences in network measures: Group differences in participant demographics (RT vs No RT vs TDC), treatment variables, and network measures were calculated using robust regressions and post hoc tests. Raw scores for network measures were mean-centered and scaled to confirm assumptions of normality prior to analyses. Diagnosis age and ICV were included as covariates in all models. Mutism, hydrocephalus, and motor deficits
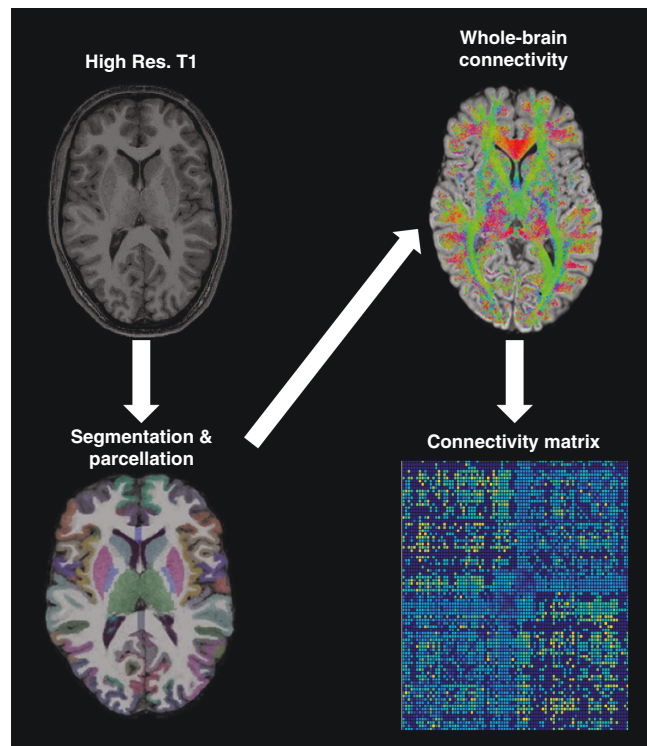

Figure 1.   High-resolution T1-weighted images were preprocessed and parcellated into cortical nodes using the Destrieux atlas in Freesurfer. DW images were preprocessed followed by constrained spherical deconvolution (CSD)-based white matter modeling and whole-brain probabilistic fiber tractography. Tractography was constrained to plausible regions using node information from parcellated T1 images. Connectivity matrices were generated with the number of streamlines connecting any 2 parcels as edge weights. DTI values were calculated for each streamline as used as edge weights in DTI connectomes. DTI, diffusion tensor imaging; DW, diffusion-weighted.

were also included as covariates to account for differences in perioperative complications across patients. A time since treatment term was included to account for variability in treatment-related neurotoxicity since treatment. Group differences were analyzed using the following model:

$$\text{graph} \quad \text{measure} = \text{group } (RT\ vs\ No\ RT\ vs\ TDC)$$
$$+ \text{diagnosis age}$$
$$+ \text{time since treatment} + \text{ICV}$$
$$+ \text{mutism} + \text{hydrocephalus} + \text{motor deficits} + \varepsilon$$

Dummy variables were entered for the TDC group for all clinical covariates.

Differences in hub organization and regional WM microstructure: Hubs were defined as brain regions in the top 15% of betweenness centrality values.[16] To enable comparisons to the TDC group, hubs in PBT survivors were defined as nodes with betweenness centrality values greater than the lowest value of the top 15% betweenness centrality values in the TDC group. We defined the most salient hubs as regions with betweenness centrality values greater than 1 standard deviation from the mean betweenness centrality value in the TDC group. We defined the most salient hubs as regions with betweenness centrality values greater than 1 standard deviation from the mean betweenness centrality value in the TDC group. Group differences (RT vs No RT vs TDC) in centrality measures for these hubs were calculated using the following model:

$$\text{centrality} = \text{group} + \text{ICV} + \varepsilon$$

Differences in the WM microstructure of salient hubs were assessed by tracing connections from hubs to all other brain regions and averaging the corresponding DTI indices across all connections. Group differences in hub connectivity were assessed using the following model:

$$\text{DTI metric} = \text{group} + \text{ICV} + \varepsilon$$

Effect of RT on the whole-brain WM network: To test the hypothesis that larger RT dose and field resulted in greater network compromise, the RT group was stratified based on treatment intensity: a *least intensive therapy* (LiT) group comprising patients that received a reduced craniospinal RT dose plus a tumor bed boost, and an *all other therapies* (AoT) group comprising patients that received all other RT treatments.[5] Differences in network measures between the LiT and AoT groups were analyzed using the robust regression model described above with a substitution for the group variable (LiT vs AoT in place of RT vs No RT vs TDC). FDR corrections for multiple comparisons were applied as previously described.

Results

Demographic and Clinical Comparisons

There were no differences in sex ($P = .49$), handedness ($P = .07$), and age at study ($P = .55$) among all 3 groups (Table 1). There were no differences in age at diagnosis ($P = .91$), time since diagnosis ($P = .42$), gross total resected tumor ($P = .89$), hydrocephalus ($P = .12$), motor deficits ($P = .11$), and mutism ($P = .19$), between the RT and No RT groups.

Group Differences in Network Measures

Small-worldness: Higher clustering coefficients were observed for real networks compared with degree-matched random networks ($C_{REAL} = 0.912$, SE $= 0.032$; $C_{RANDOM} = 0.266$, SE $= 0.004$). Approximately similar characteristic path lengths were observed for both real and random networks ($L_{REAL} = 2.284$, SE $= 0.009$; $L_{RANDOM} = 1.76$, SE $= 0.008$). Small-world organization was confirmed for all 3 groups ($C_{REAL} > C_{RANDOM}$; $L_{REAL} \approx L_{RANDOM}$) and a significant effect of group on small-worldness was observed [$F(2, 79) = 4.78$, $q < 0.05$] (Figure 2). Post hoc comparisons indicated that small-worldness was greater in the RT group compared to the TDC group (RT mean $= 2.84$, TDC mean $= 2.79$; adj. $P = .019$).

Integration: No differences in characteristic path length or global efficiency were observed (Figure 2). A trend for longer path lengths ($P = .036$) and lower global efficiency ($P = .037$) was observed in PBT survivors, however it did not survive corrections for multiple comparisons (Supplementary Table 2).

Segregation: When compared with the TDC group, the RT group demonstrated greater clustering coefficient (RT$_{mean} = 3.08$; TDC$_{mean} = 3.00$, adj. $P = .015$), local efficiency (RT$_{mean} = 1.09$; TDC$_{mean} = 1.08$, adj. $P = .003$), and modularity (RT$_{mean} = 0.50$; TDC$_{mean} = 0.47$, adj. $P = .00009$). The No RT group did not differ from the RT or TDC groups on any of these measures (Figure 2).

Centrality: There was a significant effect of group on the network-averaged participation coefficient [$F(2, 79) = 5.91$, $q < 0.05$]. Compared to the TDC group, mean participation coefficient was significantly lower in the RT (RT$_{mean} = 0.555$, TDC$_{mean} = 0.598$; adj. $P = .015$) and No RT groups (No RT$_{mean} = 0.559$, TDC$_{mean} = 0.598$; adj. $P = .042$).

Hub Distribution and Regional Relationships With WM Microstructure

Four brain regions were identified as hubs in the TDC group but not in patients (Table 2). One region, the superior segment of the circular sulcus of the insular, was a hub in PBT survivors but not in the TDC group (Table 2). The right hemisphere pericallosal sulcus, left hemisphere pericallosal sulcus, and right hemisphere parietooccipital sulcus were identified as the most salient hubs in all groups (Figure 3). A fourth region, the left parietooccipital sulcus, was identified as a salient hub in the TDC group but not in survivors (Figure 3). The bilateral calcarine sulci and the left hemisphere inferior segment of the insular sulcus were identified as additional hubs in the No RT group, while the left hemisphere calcarine sulcus was identified as an additional hub in the RT group (Figure 3).

Differences in microstructure for WM traced from hubs were observed (Figure 4). For WM from the pericallosal sulcus in the left hemisphere, there was a main effect of group on FA [$F(2, 79) = 4.97$, $q < 0.01$], MD [$F(2, 79) = 11.02$,
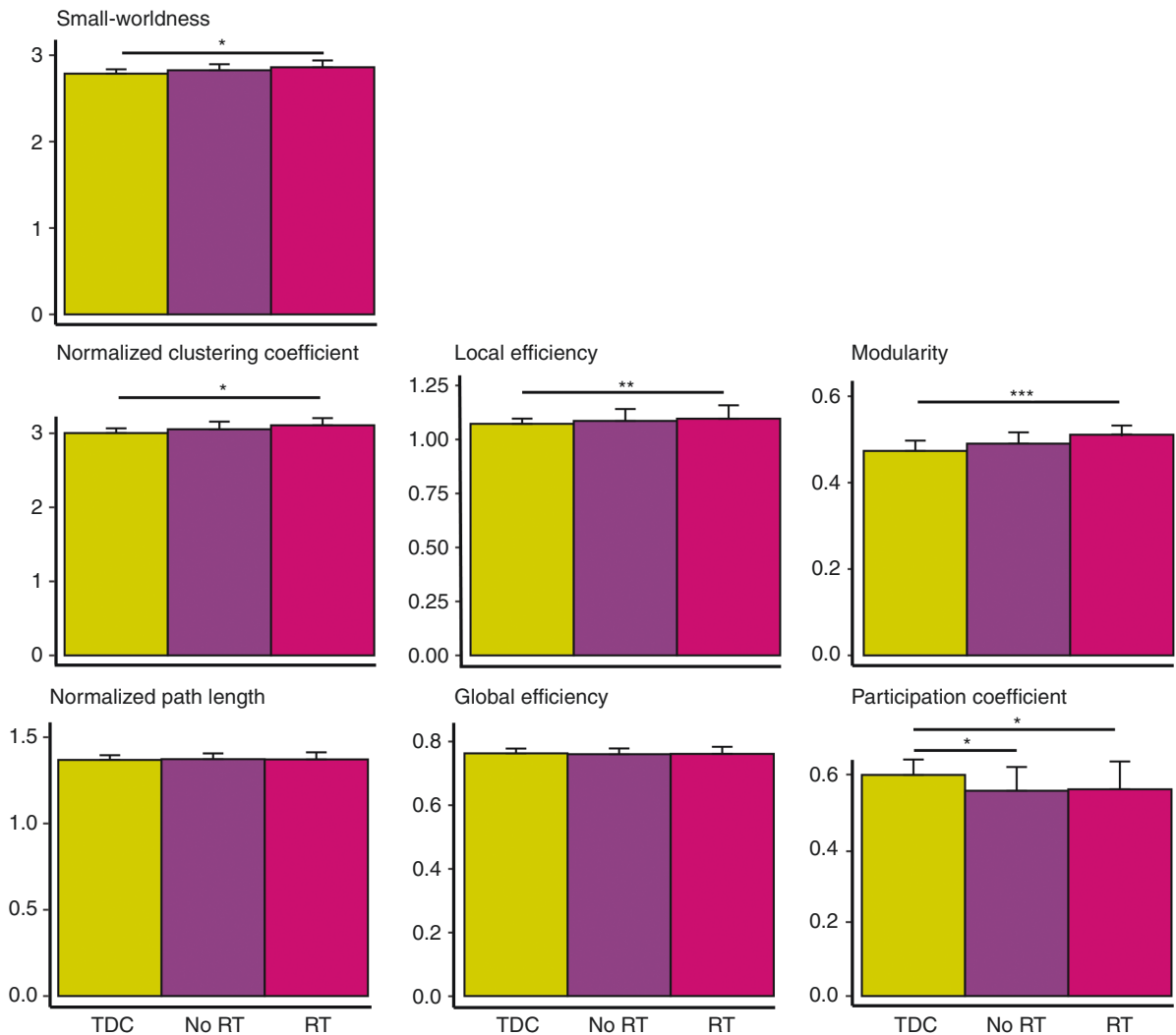
Figure 2. Group differences in network measures. Adjusted *P* values are denoted as **P* < .05, ***P* < .001, ****P* < .0001. The error bars indicate standard deviation. No RT, no radiation therapy; RT, radiation therapy; TDC, typically developing children.

q < 0.0001], AD [*F*(2, 79) = 10.00, *q* < 0.0001], and RD [*F*(2, 79) = 8.53, *q* < 0.0001]. WM from the pericallosal sulcus in the right hemisphere showed a main effect of group on FA [*F*(2, 79) = 8.87, *q* < 0.0001 and RD [*F*(2, 79) = 8.27, *q* < 0.001]. A main effect of group on MD [*F*(2, 79) = 5.78, *q* < 0.05] and RD [*F*(2, 79) = 5.12, *q* < 0.05] for WM from the parietooccipital sulcus in the right hemisphere was observed. Post hoc analyses revealed compromised WM from these regions in PBT survivors. When compared to the TDC group, the RT group showed lower FA (*t* = −3.25, adj. *P* < .01), and higher MD (*t* = 4.88, adj. *P* < .001), AD (*t* = 3.95, adj. *P* < .001), and RD (*t* = 3.28, adj. *P* < .01) of WM from the pericallosal sulcus in the left hemisphere. Likewise, the No RT group showed lower FA (*t* = −2.44, adj. *P* < .05), and higher MD (*t* = 3.27, adj. *P* < .001), AD (*t* = 3.06, adj. *P* < .01), and RD (*t* = 3.28, adj. *P* < .01) of these tracts when compared to the TDC group. The RT group showed lower FA (*t* = −4.82, adj. *P* < .001) and higher RD (*t* = 4.30, adj. *P* < .001) of WM from the pericallosal sulcus in the right

hemisphere compared to the TDC group. The RT group also showed higher MD (*t* = 3.27, adj. *P* < .01) and RD (*t* = 2.94, adj. *P* < .01) of WM from the parietooccipital sulcus in the right hemisphere, while the No RT group showed higher RD (*t* = 2.55, adj. *P* < .05) of these tracts compared to the TDC group. There were no differences in the centrality measures of these hubs (Supplementary Figure 1).

Associations Between RT and Network Measures

Network measures were compared between those that received less intensive radiation treatment (LiT) and those that received more aggressive radiation treatment (AoT). Significant pairwise differences were observed for normalized shortest path length (AoT > LiT; *P* = .041), global efficiency (AoT < LiT; *P* = .032), and betweenness centrality (AoT > LiT; *P* = .036). However, these differences did not survive corrections for multiple comparisons (Supplementary Table 3).

Table 2. Hub regions of structural brain networks in typically developing children and pediatric brain tumor survivors

Regions identified as hubs	TDC		No RT		RT	
	Hub?	B_c	Hub?	B_c	Hub?	B_c
Left hemisphere						
Pericallosal sulcus	+	1630	+	1440	+	1840
Parieto-occipital sulcus	+	260	+	229	+	236
Inferior segment of the circular sulcus of the insular	+	246	+	257	+	216
Calcarine sulcus	+	241	+	294	+	264
Intraparietal sulcus and transverse parietal sulcus	+	183	+	153	+	160
Superior temporal sulcus	+	161	+	145	+	172
Posterior segment of the lateral sulcus	+	143	+	130	+	176
Superior segment of the circular sulcus of the insular	+	123	+	140	+	201
Subcallosal gyrus	+	132	+	125	–	—
Superior frontal gyrus	+	117	+	—	–	—
Long insular gyrus and central sulcus of the insular	+	107	–	—	–	—
Superior occipital sulcus and transverse occipital sulcus	+	104	–	—	–	—
Right hemisphere						
Pericallosal sulcus	+	1480	+	1510	+	1700
Parieto-occipital sulcus	+	270	+	312	+	271
Calcarine sulcus	+	223	+	256	+	237
Intraparietal sulcus and transverse parietal sulcus	+	217	+	124	+	199
Inferior segment of the circular sulcus of the insular	+	200	+	217	+	207
Superior temporal sulcus	+	170	+	171	+	208
Posterior segment of the lateral sulcus	+	165	+	183	+	197
Anterior cingulate gyrus and sulcus	+	108	+	130	+	114
Superior frontal gyrus	+	110	+	—	–	—
Superior occipital sulcus and transverse occipital sulcus	+	124	–	—	+	112
Superior segment of the circular sulcus of the insular	–	—	+	104	+	121

Hub regions were identified if average nodal B_c was within the top 15% of all B_c values in the TDC group. The B_c value represents the AUC value of betweenness centrality across all thresholds. (+) denotes regions identified as hubs and (–) denotes regions not identified as hubs in each group. Group differences are bolded. AUC, area under the curve; RT, radiotherapy; TDC, typically developing children.
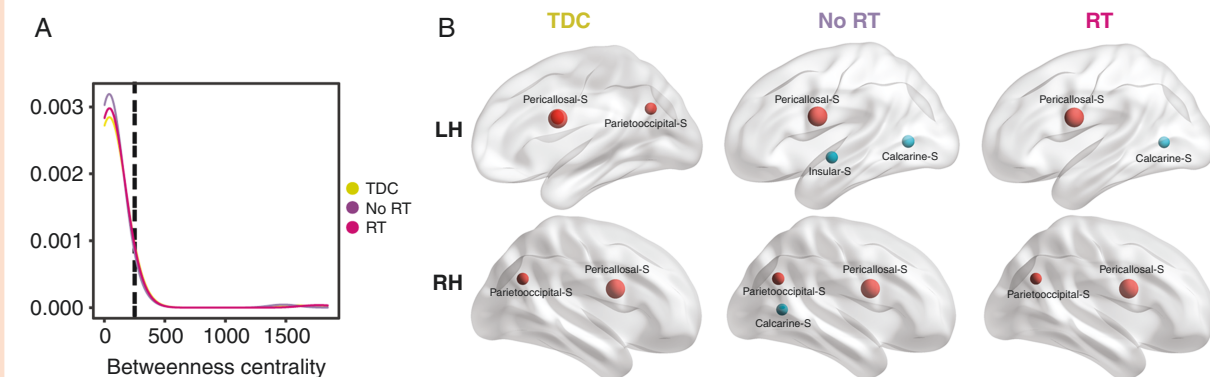

Figure 3. (a) The distribution of betweenness centrality in each group of participants. Betweenness centrality for a vast majority of nodes was less that 1 standard deviation from the mean centrality value in typically-developing children (dashed line). Nodes with betweenness centrality values greater than this boundary were identified as hub regions. (b) Identification of hub regions in each group of participants. The size of the hub denotes its betweenness centrality value. The pericallosal sulcus bilaterally and the parieto-occipital sulcus in the right hemisphere are hubs common to all participants. The calcarine sulcus bilaterally and the insular sulcus in the left hemisphere are hubs identified only in patients. LH, left hemisphere; No RT, no radiation therapy; RH, right hemisphere; RT, radiation therapy; TDC, typically-developing children.
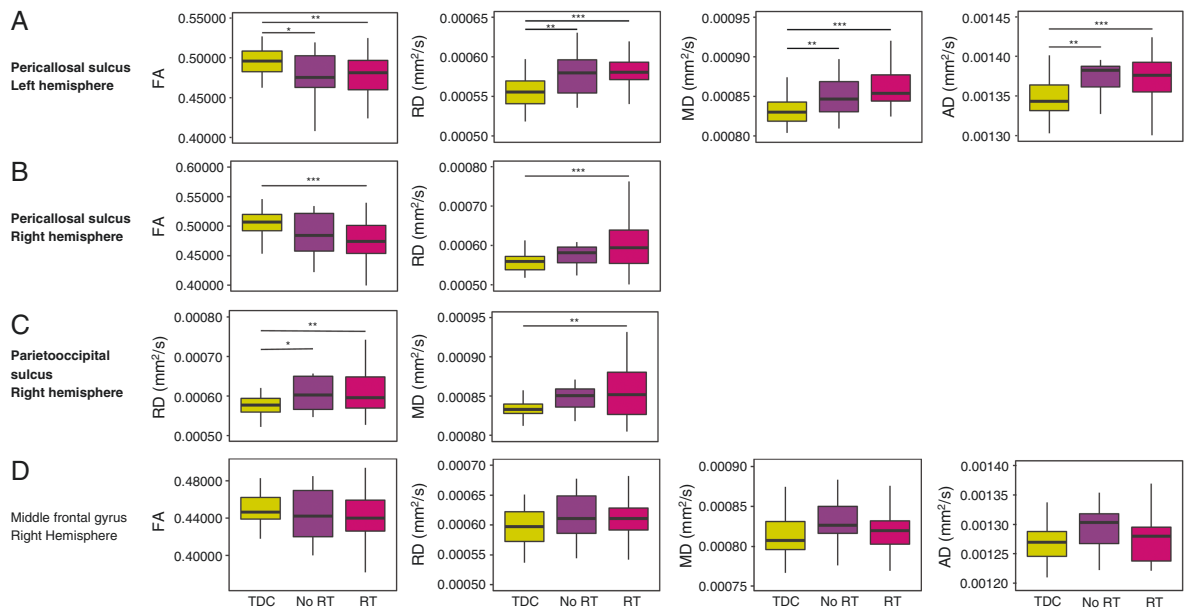
Figure 4. Group differences in the average nodal DTI index for hub regions common to all participants. Hub regions are bolded. (a) Significant pairwise differences between typically developing children and both survivor groups were observed for average nodal DTI indices from the pericallosal sulcus in the left hemisphere. (b) Significant differences were observed between typically developing children and survivors in the RT group for average nodal FA and RD of the pericallosal sulcus in the right hemisphere. (c) Group differences were also observed for average nodal RD and MD of the parietooccipital sulcus in the right hemisphere. (d) There were no differences in average nodal DTI indices of a non-hub region (middle frontal gyrus; not bolded). Adjusted P values are denoted as $*P < .05$, $**P < .001$, $***P < .0001$. AD, axial diffusivity; DTI, diffusion tensor imaging; FA, fractional anisotropy; MD, mean diffusivity; No RT, no radiation therapy; RD, radial diffusivity; RT, radiation therapy; TDC, typically developing children.

Age and Brain Volume Are Correlated With Local Efficiency of Structural Networks

The local efficiencies of structural networks were significantly correlated with age at study and ICV (Supplementary Figure 2). Increasing age was associated with decreasing local efficiency in all 3 groups ($\beta = -0.0004$, $t(79) = -2.26$, $P = .03$). Larger brain volumes were associated with greater local efficiency of structural networks ($\beta = 1.14 \times 10^{-8}$, $t(79) = 3.27$, $P = .002$).

Discussion

In this study, we examined whether structural network connectivity is affected by curative brain tumor treatment—a model of pediatric brain injury. PBT and TDC groups exhibited small-world topologies, indicating that the structural networks analyzed in this study are biologically plausible. Novel to the field, we detected relatively stable integration but increased segregation of the structural connectome in children treated with RT. Clustering coefficient, local efficiency, and modularity were greater following RT treatment, whereas characteristic path length and global efficiency remained unchanged. We also identified lower network-averaged participation coefficient after treatment with or without RT. Network hubs were variably distributed among study participants, where brain areas identified as hubs in the TDC group were not identified as hubs in the

PBT survivors and vice versa. Evidence of regional WM compromise was demonstrated by lower FA and higher MD, AD, and RD of traced WM from hubs in PBT survivors. Taken together, our results describe a pediatric brain injury model that is characterized by greater network segregation and regional WM compromise of structural brain networks.

Greater segregation of whole-brain WM networks may result from RT-related alterations to the emergence and maintenance of local axonal tracts. This is based on the fact that short-range WM that subserve local network connectivity begin to develop in childhood[29] and have a protracted maturational trajectory that extends into adolescence.[30,31] RT may disrupt the physiological processes supporting local WM connectivity, including the overproduction, maintenance, and pruning of short-distance axons and their synapses. Indeed, alterations to local network connectivity have been observed in other pediatric brain injury models.[3,32] In contrast, global WM connectivity may be more resilient to the effects of RT. WM networks evolve from localized patterns of connectivity designed to support basic functions, to more distributed configurations that are favorable for higher-order cognitive processes.[33,34] Distributed configurations are supported by long-range WM connections that promote greater integration of the structural connectome from infancy and early childhood.[35–37] This suggests that global connectivity is established prior to RT treatment and thus may be more resilient to injury. Our findings are supported by prior work showing that rapidly maturing brain regions are more vulnerable to disruption after a pediatric brain injury,[38] further

indicating an increased vulnerability of rapidly maturing local network connectivity to RT.

We found structural brain networks to be more modular in children treated with RT. Networks high in modularity display greater numbers of intra- vs intermodule connections[39] and are associated with reduced capacity for whole-brain connectivity.[40] Brain networks become less modular and more integrated during development, reflecting an optimal configuration that prioritizes greater intermodule connectivity.[35] For the RT group, increased modularity and decreased participation coefficient suggests that WM networks are less optimally configured after RT, though this occurs in the context of unchanged global efficiency.

There was evidence for hub reorganization in PBT survivors. Brain networks possess heavy-tailed degree distributions where a small number of nodes account for a high degree of connectivity.[41] Hubs are centrally embedded within the network and tend to remain stable from infancy.[35] It is notable that the weakest hubs in the TDC group were most likely to be lost as network hubs in PBT survivors, suggesting that brain regions less well embedded within the structural network are more vulnerable to the effects of injury. Moreover, regions such as the superior frontal gyrus which are known network hubs were identified as hubs in the TDC group but not in PBT survivors. Highly connected regions such as the insular and calcarine sulci were identified as hubs in all participants, yet when the strongest hubs were delineated in each group, these areas remained as some of the strongest hubs in PBT survivors but not in the TDC group. These findings suggest that stronger hubs become more embedded within the structural network as weaker hubs are lost to injury. This reorganization of hub connectivity may be compensatory given that the overall *hubbiness* of the structural network remained unchanged (no group differences in betweenness centrality) while the underlying WM architecture was damaged in survivors.

Our findings are discussed in the context of the following limitations. First, though radiation therapy is strongly associated with treatment effects experienced by PBT survivors, it is by no means the only contributor to WM injury. Previous work has shown that surgery alone can impart significant damage to WM[6] and contribute to cognitive risk in brain tumor survivors through localized brain injury.[42,43] Although it is more difficult to isolate the unique impact of chemotherapy on WM injury due to its administration as adjuvant therapy, evidence suggests that brain tumor patients treated with chemotherapy-only regimens exhibit WM damage and poorer intellectual outcomes.[7,44] The unique impacts of surgery and chemotherapy will need to be considered in larger cohorts of childhood brain tumor survivors to adequately clarify the impact of PBT on WM connectivity. Second, although a multitude of methods for constructing structural connectomes from DTI data have been proposed, there are currently no standardized approaches. The choice of cortical parcellation, edge-weight definition, and thresholding scheme have a substantive impact on network measures.[45] The methods employed in this study reflect recommended practices in other clinical populations and were chosen to facilitate comparisons with other studies. Second, limitations of traditional DTI approaches can lead to the inclusion of false positive and false negative streamlines in structural connectivity matrices; to overcome this, we used a constrained deconvolution approach to model WM.[25] While useful, newer methods such as diffusion kurtosis imaging[46] may provide better delineation of WM connectivity, especially around gray matter–WM boundaries close to the cortical surface. Third, the current analyses were based on an unbalanced sample of children treated without RT (*n* = 13). It is possible that we were underpowered to detect significant pairwise effects for this cohort of survivors, which may explain why we observed fewer significant network differences in this group. A larger sample of survivors treated without RT is required to clarify the findings from this study. Fourth, given our cross-sectional study, we were precluded from assessing age-related effects on modular organization. Future studies assessing the impact of treatment on a priori defined modules as well as those employing a longitudinal design, will better clarify the impact of pediatric brain injury on the modular organization of structural brain networks.

Supplementary Material

Supplementary material is available at *Neuro-Oncology Advances* online.

Supplementary Figure 1. Group differences in measures of centrality for hub regions common to all participants. There were no significant differences in betweenness centrality (Bc), degree centrality (Dc), and participation coefficient (Pc) among groups. *P* values and FDR-corrected *P* values (*q*) are bolded.

Supplementary Figure 2. Age at study and intracranial volume (ICV) predicted the local efficiency of structural networks. Older age at study was associated with lower local efficiencies while larger brain volumes were predictive of greater local efficiency of structural networks. No RT, no radiation therapy; RT, radiation therapy; TDC, typically developing children.

Keywords

brain connectivity | brain tumor | graph theory | structural connectome | white matter.

Conflict of interest statement. None declared.

Authorship Statement. Study conception and design: A.O. and D.J.M. Provision of study materials and patients: E.B., M.T., V.R., S.L., and D.J.M. Collection and assembly of data: A.O., I.M.-E., K.B., and J.S. Analysis and interpretation: all authors. Writing and final approval of the manuscript: all authors.

References

1. Sharp DJ, Scott G, Leech R. Network dysfunction after traumatic brain injury. *Nat Rev Neurol.* 2014;10(3):156–166.

2. Caeyenberghs K, Leemans A, De Decker C, et al. Brain connectivity and postural control in young traumatic brain injury patients: a diffusion MRI based network analysis. *Neuroimage Clin.* 2012;1(1):106–115.

3. Yuan W, Wade SL, Babcock L. Structural connectivity abnormality in children with acute mild traumatic brain injury using graph theoretical analysis. *Hum Brain Mapp.* 2015;36(2):779–792.

4. Nieman BJ, Elizabeth De Guzman A, Gazdzinski LM, et al. White and gray matter abnormalities after cranial radiation in children and mice [published online ahead of print 2015]. *Int J Radiat Oncol Biol Phys.* 93(4):882–891.

5. Moxon-Emre I, Bouffet E, Taylor MD, et al. Vulnerability of white matter to insult during childhood: evidence from patients treated for medulloblastoma. *J Neurosurg Pediatr.* 2016;18(1):29–40.

6. Liu F, Scantlebury N, Tabori U, et al. White matter compromise predicts poor intellectual outcome in survivors of pediatric low-grade glioma. *Neuro Oncol.* 2014;17(4):604–613.

7. Riva D, Giorgi C, Nichelli F, et al. Intrathecal methotrexate affects cognitive function in children with medulloblastoma. *Neurology.* 2002;59(1):48–53.

8. Rubinov M, Sporns O. Complex network measures of brain connectivity: uses and interpretations. *Neuroimage.* 2010;52(3):1059–1069.

9. Honey CJ, Kötter R, Breakspear M, Sporns O. Network structure of cerebral cortex shapes functional connectivity on multiple time scales. *Proc Natl Acad Sci U S A.* 2007;104(24):10240–10245.

10. Baum GL, Ciric R, Roalf DR, et al. Modular segregation of structural brain networks supports the development of executive function in youth. *Curr Biol.* 2017;27(11):1561–1572.e8.

11. Bathelt J, Gathercole SE, Butterfield S, Astle DE. Children's academic attainment is linked to the global organization of the white matter connectome. *Dev Sci.* 2018;21(5):e12662.

12. Rudie JD, Brown JA, Beck-Pancer D, et al. Altered functional and structural brain network organization in autism. *Neuroimage Clin.* 2013;2:79–94.

13. Lim S, Han CE, Uhlhaas PJ, Kaiser M. Preferential detachment during human brain development: age- and sex-specific structural connectivity in diffusion tensor imaging (DTI) data. *Cereb Cortex.* 2015;25(6):1477–1489.

14. Severino M, Tortora D, Toselli B, et al. Structural connectivity analysis in children with segmental callosal agenesis. *Am J Neuroradiol.* 2017;38(3):639–647.

15. Bathelt J, Scerif G, Nobre AC, Astle DE. Whole-brain white matter organization, intelligence, and educational attainment. *Trends Neurosci Educ.* 2019;15:38–47.

16. Cao Q, Shu N, An L, et al. Probabilistic diffusion tractography and graph theory analysis reveal abnormal white matter structural connectivity networks in drug-naive boys with attention deficit/hyperactivity disorder. *J Neurosci.* 2013;33(26):10676–10687.

17. Le Bihan D, Mangin JF, Poupon C, et al. Diffusion tensor imaging: concepts and applications. *J Magn Reson Imaging.* 2001;13(4):534–546.

18. Beaulieu C. The basis of anisotropic water diffusion in the nervous system—a technical review. *NMR Biomed.* 2002;15(7–8):435–455.

19. Scantlebury N, Bouffet E, Laughlin S, et al. White matter and information processing speed following treatment with cranial-spinal radiation for pediatric brain tumor. *Neuropsychology.* 2016;30(4):425–438.

20. Nieman BJ, Elizabeth De Guzman A, Gazdzinski LM, et al. White and gray matter abnormalities after cranial radiation in children and mice. *Int J Radiat Oncol Biol Phys.* 2015;93(4):882–891.

21. Glass JO, Ogg RJ, Hyun JW, et al. Disrupted development and integrity of frontal white matter in patients treated for pediatric medulloblastoma. *Neuro Oncol.* 2017;19(10):1408–1418.

22. Fischl B. FreeSurfer. *Neuroimage.* 2012;62(2):774–781.

23. Destrieux C, Fischl B, Dale A, Halgren E. Automatic parcellation of human cortical gyri and sulci using standard anatomical nomenclature. *Neuroimage.* 2010;53(1):1–15.

24. Jenkinson M, Woolrich MW, Beckmann CF, et al. Advances in functional and structural MR image analysis and implementation as FSL. *Neuroimage.* 2004;23(suppl 1):S208–S219.

25. Tournier JD, Smith R, Raffelt D, et al. MRtrix3: a fast, flexible and open software framework for medical image processing and visualisation. *Neuroimage.* 2019;202:1–17.

26. Drakesmith M, Caeyenberghs K, Dutt A, et al. Overcoming the effects of false positives and threshold bias in graph theoretical analyses of neuroimaging data. *Neuroimage.* 2015;118:313–333.

27. Rubinov M, Knock SA, Stam CJ, et al. Small-world properties of nonlinear brain activity in schizophrenia. *Hum Brain Mapp.* 2009;30(2):403–416.

28. Wang J, Wang X, Xia M, et al. GRETNA: a graph theoretical network analysis toolbox for imaging connectomics. *Front Hum Neurosci.* 2015;9:1–16.

29. Innocenti GM, Price DJ. Exuberance in the development of cortical networks. *Nat Rev Neurosci.* 2005;6(12):955–965.

30. Wu M, Lu LH, Lowes A, et al. Development of superficial white matter and its structural interplay with cortical gray matter in children and adolescents. *Hum Brain Mapp.* 2014;35(6):2806–2816.

31. Oyefiade AA, Ameis S, Lerch JP, et al. Development of short-range white matter in healthy children and adolescents. *Hum Brain Mapp.* 2018;39(1):204–217.

32. Ewing-Cobbs L, Johnson CP, Juranek J, et al. Longitudinal diffusion tensor imaging after pediatric traumatic brain injury: impact of age at injury and time since injury on pathway integrity. *Hum Brain Mapp.* 2016;37(11):3929–3945.

33. Yap PT, Fan Y, Chen Y, et al. Development trends of white matter connectivity in the first years of life. *PLoS One.* 2011;6(9):e24678.

34. Chen Z, Liu M, Gross DW, Beaulieu C. Graph theoretical analysis of developmental patterns of the white matter network. *Front Hum Neurosci.* 2013;7:1–13.

35. Hagmann P, Sporns O, Madan N, et al. White matter maturation reshapes structural connectivity in the late developing human brain. *Proc Natl Acad Sci U S A.* 2010;107(44):19067–19072.

36. Dennis EL, Jahanshad N, McMahon KL, et al. Development of brain structural connectivity between ages 12 and 30: a 4-Tesla diffusion imaging study in 439 adolescents and adults. *Neuroimage.* 2013;64:671–684.

37. Tymofiyeva O, Hess CP, Ziv E, et al. A DTI-based template-free cortical connectome study of brain maturation. *PLoS One.* 2013;8(5):e63310.

38. Babikian T, Merkley T, Savage RC, Giza CC, Levin H. Chronic aspects of pediatric traumatic brain injury: review of the literature. *J Neurotrauma.* 2015;32(23):1849–1860.

39. Newman MEJ, Girvan M. Finding and evaluating community structure in networks. *Phys Rev E Stat Nonlinear Soft Matter Phys.* 2004;69(2):026113.

40. Crossley NA, Mechelli A, Vértes PE, et al. Cognitive relevance of the community structure of the human brain functional coactivation network. *Proc Natl Acad Sci U S A.* 2013;110(28):11583–11588.

41. van den Heuvel MP, Sporns O. Network hubs in the human brain. *Trends Cogn Sci.* 2013;17(12):683–696.

42. Ris MD, Beebe DW, Armstrong FD, et al. Cognitive and adaptive outcome in extracerebellar low-grade brain tumors in children: a report from the Children's Oncology Group. *J Clin Oncol.* 2008;26(29):4765–4770.

43. Fouladi M, Wallace D, Langston JW, et al. Survival and functional outcome of children with hypothalamic/chiasmatic tumors. *Cancer.* 2003;97(4):1084–1092.

44. Aukema EJ, Caan MWA, Oudhuis N, et al. White matter fractional anisotropy correlates with speed of processing and motor speed in young childhood cancer survivors. *Int J Radiat Oncol Biol Phys.* 2009;74(3):837–843.

45. Proix T, Spiegler A, Schirner M, et al. How do parcellation size and short-range connectivity affect dynamics in large-scale brain network models? *Neuroimage.* 2016;142:135–149.

46. Jensen JH, Helpern JA, Ramani A, Lu H, Kaczynski K. Diffusional kurtosis imaging: the quantification of non-Gaussian water diffusion by means of magnetic resonance imaging. *Magn Reson Med.* 2005;53(6):1432–1440.